Journal of Power Sources 249 (2014) 231–238

Contents lists available at ScienceDirect

Journal of Power Sources

journal homepage: www.elsevier.com/locate/jpowsour

Electro-thermal analysis of Lithium Iron Phosphate battery for electric vehicles

L.H. Saw, K. Somasundaram, Y. Ye, A.A.O. Tay*

Department of Mechanical Engineering, Faculty of Engineering, National University of Singapore, Singapore 117576, Singapore

HIGHLIGHTS

- We modeled the electrical and thermal behavior of the Li-ion battery.
- We analyzed the dynamic behavior of the cell using SFUDS cycle.
- We carried out experimental study to validate the simulation results.
- We studied the thermal response of the battery pack under different driving cycle.
- Heat generation of the battery pack is the highest for US06 cycle.

ARTICLE INFO

Article history:
Received 13 August 2013
Received in revised form
4 October 2013
Accepted 14 October 2013
Available online 25 October 2013

Keywords:
Battery temperature
Electric vehicles
Electro-thermal model
Heat generation
Lithium Iron Phosphate battery

ABSTRACT

Lithium ion batteries offer an attractive solution for powering electric vehicles due to their relatively high specific energy and specific power, however, the temperature of the batteries greatly affects their performance as well as cycle life. In this work, an empirical equation characterizing the battery's electrical behavior is coupled with a lumped thermal model to analyze the electrical and thermal behavior of the 18650 Lithium Iron Phosphate cell. Under constant current discharging mode, the cell temperature increases with increasing charge/discharge rates. The dynamic behavior of the battery is also analyzed under a Simplified Federal Urban Driving Schedule and it is found that heat generated from the battery during this cycle is negligible. Simulation results are validated with experimental data. The validated single cell model is then extended to study the dynamic behavior of an electric vehicle battery pack. The modeling results predict that more heat is generated on an aggressive US06 driving cycle as compared to UDDS and HWFET cycle. An extensive thermal management system is needed for the electric vehicle battery pack especially during aggressive driving conditions to ensure that the cells are maintained within the desirable operating limits and temperature uniformity is achieved between the cells.

1. Introduction

The world relies heavily on fossil fuel to meet the daily power demands, ranging from electricity generation to transportation. In 2009, the logistics sector had contributed to 61.7% of the total world oil consumption and 23% of the total world CO_2 emission [1]. With advances in battery technology, concerns on global warming and increasing fuel prices, automotive manufacturers are forced to shift their attention to electric vehicles (EVs). EVs are more energy efficient and cleaner than conventional Internal Combustion Engine (ICE) vehicles and are projected as the most sustainable solutions for the future transport [1–3], however, the success of EVs depends on the development of the battery.

Lithium-ion batteries provide an attractive solution for EVs due to its high power and energy density, however, thermal issues in Li-ion batteries have to be addressed to make them safer, reliable and last longer for high power applications. Bandhaeur et al. [4] have provided a detailed review of the thermal issues in Li-ion batteries. Safety, cycle life and capacity retention are some of the major aspects affected by the operating temperature. Hence, a control and management of the thermal envelope is required to have a safer and reliable operation of a Li-ion battery.

Various test procedures used to investigate the performance, reliability and safety of Li-ion batteries are documented in ISO 12405-1/2, IEC 62660-1/2 [3]. In order to design a realistic thermal management system for EVs, it is also important to characterize the

* Corresponding author. Department of Mechanical Engineering, National University of Singapore, EA-07-19, 9 Engineering Drive 1, Singapore 117575, Singapore. Tel.: +65 65162207; fax: +65 67791459.
E-mail addresses: bernardsaw@nus.edu.sg (L.H. Saw), mpetayao@nus.edu.sg (A.A.O. Tay).

0378-7753/$ – see front matter © 2013 Elsevier B.V. All rights reserved.
http://dx.doi.org/10.1016/j.jpowsour.2013.10.052

Nomenclature

A	exponential voltage, V
A_s	external surface area of the cell, m^2
A_{mf}	cross section flow area for cooling air per module, m^2
A_{ms}	total module surface area exposed to cooling air, m^2
B	exponential zone time constant, $(Ah)^{-1}$
C_p	specific heat capacity of the battery, J kg^{-1} K^{-1}
C_{bp}	theoretical capacity of the battery, Ah
E	emissivity
E_0	constant voltage, V
h	convective heat transfer coefficient, W m^{-2} K^{-1}
I_{dis}	discharge current, A
i	current, A
i^*	filtered current, A
K	polarization constant, $V(Ah)^{-1}$ or polarization resistance, Ω
$\dot{m}$	mass flow rate of air, kg s^{-1}
Q	capacity, Ah
R	internal resistance, Ω
R_c	terminal contact resistance, Ω
T_{dis}	discharge time, h
T_{module}	module temperature, K
T_{surf}	surface temperature of battery, K
T_∞	free stream temperature of air, K
t	time, s
V_{batt}	voltage, V
ρ	density of the battery, kg m^{-3}
ρ_{air}	density of the air, kg m^{-3}
σ_{sb}	Stefan–Boltzmann constant, W m^{-2} K^{-4}

Subscript

exp	exponential
nom	nominal
full	fully charged
max	maximum

Superscripts

k	Peukert constant

thermal phenomena of Li-ion cell for the required transient power response. Among the various driving cycles, Simplified Federal Urban Driving Schedule (SFUDS) has been widely used to evaluate the power delivery capability and cycle life of the cell at laboratory level [5–7], however, the facility needed to carry out the testing of the EV battery packs such as high power programmable battery cycler is always expensive and requires several hundred hours of testing. The battery pack may not be comprehensively tested due to the limitations of the battery cycler.

Numerical modeling could be used to overcome the limitations in battery testing. Numerical modeling not only helps to improve the understanding of the battery operating mechanism but also provides internal information that are difficult to obtain through experiments such as electrochemical reaction rates inside the cell, heat generation, temperature distribution, voltage distribution, current distribution, etc. Various mathematical models have been used to investigate the thermal response of the battery such as empirical equations [7], electrochemical models [8–12], RC models [13–15], and lumped parameter models [16,17]. Although electrochemical models can predict the aging and thermal behavior of the Li-ion battery, coupled time variant spatial partial differential equations make them complex and their solution demands extensive computational resources [18]. Besides, most of the studies only presented a numerical simulation results and doesn't compare with the experimental work [4,19–22]. Various types of thermal management systems such as air cooling [23–25], liquid cooling [26,27] and phase change material [28–30] technologies have been proposed to maintain the batteries at the optimum operating temperature at both cell and pack levels [31].

In view of the challenges in experimental testing and detailed modeling, the objective of this work is twofold. First, an empirical equation coupled with a lumped thermal model has been used to predict the cell voltage, heat generation, temperature rise of the cell during constant-current discharging and SFUDS cycle for an 18650 Lithium Iron Phosphate (LFP) cell and is validated with experiments; and second, to apply the validated single cell model to investigate the thermal response of the battery pack of a converted EV under Urban Dynamometer Driving Schedule (UDDS), Highway Fuel Economy Driving Schedule (HWFET) and US06 Supplemental Federal Test Procedure (SFTP) driving cycles. The results are discussed in terms of the total heat generated during these driving cycles and the evolution of the battery pack temperature under a forced convection cooling system.

2. Mathematical model

2.1. The battery model

A battery model is needed to define its voltage in terms of current and state of charge (SOC). In this study, modified Shepherd model has been employed to represent the voltage dynamics of the LFP cell [32–34]. A typical discharge curve of the Li-ion battery is shown in Fig. 2. The discharge curve of the Li-ion battery can be divided into three sections. The first section represents the exponential potential drop of the cell during initial discharge. The second section represents the amount of charge that can be extracted from the cell before reaching the nominal voltage of the cell. The last section represents the total discharge of the cell, when the voltage of the cell drops rapidly to the cut off voltage. The modified Shepherd equation for charging and discharging is given by Eqs. (1) and (2) respectively [32–34]. It is assumed that the internal resistance of the cell is constant throughout the charging and discharging cycle and doesn't change with the I_t-rates. The temperature effect on the battery model behavior is neglected and the model parameters for discharging and charging are identical.

Charging ($i^* < 0$)

$$V_{batt} = E_0 - R\cdot i - K\frac{Q}{it - 0.1\cdot Q}\cdot i^* - K\left(\frac{Q}{Q - it}\right)it + A\exp(-B\cdot it) \quad (1)$$

Discharging ($i^* > 0$)

$$V_{batt} = E_0 - R\cdot i - K\frac{Q}{Q - it}\cdot i^* - K\left(\frac{Q}{Q - it}\right)it + A\exp(-B\cdot it) \quad (2)$$

The voltage of the cell at a fully charged state is defined in Eq. (3) [33,34].

$$V_{full} = E_0 - R\cdot i + A \quad (3)$$

The voltage at the exponential section is defined in Eq. (4) [33,34].

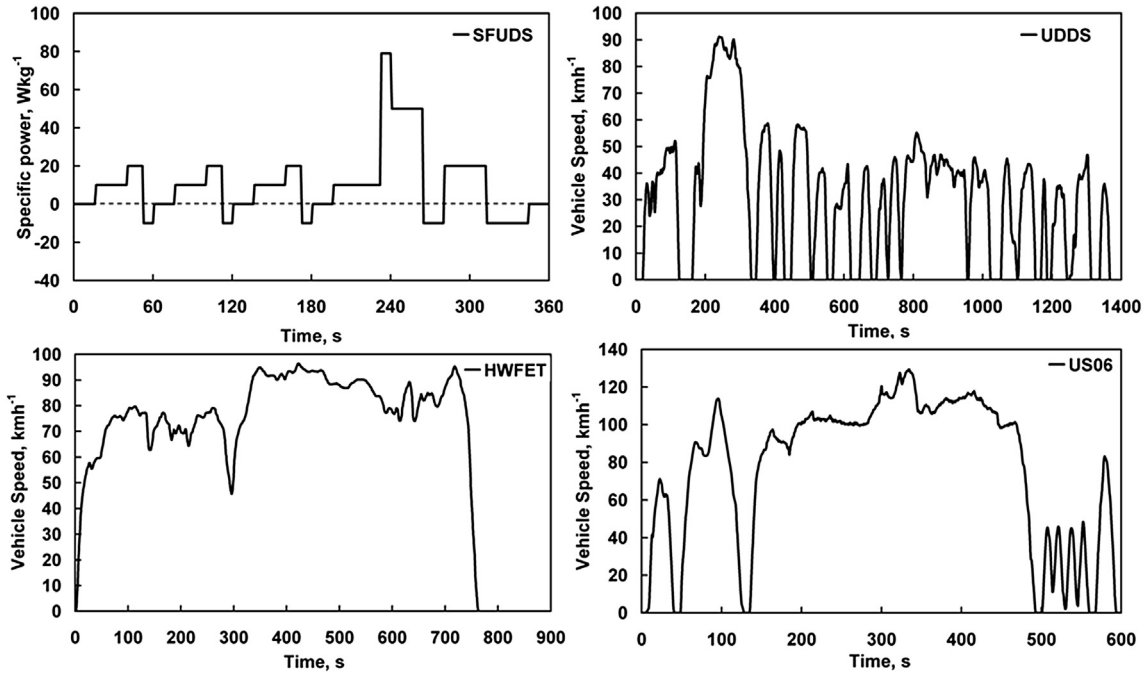

Fig. 1. Testing cycle for single cell and EV battery pack.

$$V_{\text{exp}} = E_0 - K\frac{Q}{Q - Q_{\text{exp}}}\cdot(Q_{\text{exp}} + i) - R\cdot i + A\exp\left(\frac{-3}{Q_{\text{exp}}}\cdot Q_{\text{exp}}\right) \tag{4}$$

The voltage of the cell at the nominal zone is defined in Eq. (5) [33,34].

$$V_{\text{nom}} = E_0 - K\frac{Q}{Q - Q_{\text{nom}}}\cdot(Q_{\text{nom}} + i) - R\cdot i + A\exp\left(\frac{-3}{Q_{\text{exp}}}\cdot Q_{\text{nom}}\right) \tag{5}$$

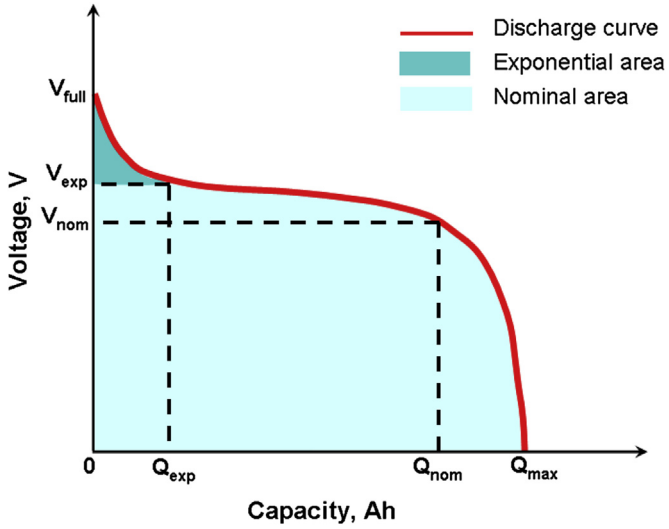

Fig. 2. Typical discharge characteristic of Li-ion battery [33,34].

2.2. Thermal model

It is assumed that the resistance to conduction within the battery is much less than the resistance to convection outside the battery surface. Therefore, the temperature inside the cell is fairly uniform [35]. Besides, it is also assumed that the physical properties of the cell are uniform and are not affected significantly by temperature. The battery model is coupled with a lumped thermal model to determine the heat generation and the average surface temperature of the cell. A general energy balance equation used to model the battery system is defined in Eq. (6) [7].

$$\rho C_{\text{p}}\frac{\text{d}T_{\text{surf}}}{\text{d}t} = Q_{\text{gen}} - hA_{\text{s}}\left(T_{\text{surf}} - T_{\infty}\right) - E\sigma_{\text{sb}}\left(T_{\text{surf}}^4 - T_{\infty}^4\right) \tag{6}$$

The heat generation in the Li-ion battery constitutes of ohmic heat, irreversible heat and reversible heat [36]. Reaction heat or irreversible heat generation is due to the transfer of electrons to or from the electrode during the electrochemical reaction, reversible heat generation is because of the entropy changes of cathode and anode, and ohmic heat generation is due to the ohmic resistance of the solid active materials and electrolyte. The entropy change in the electrodes is related to the change of their equilibrium potential with temperature ($\text{d}U/\text{d}T$) and this varies with SOC. Here, this relation is adopted from the work of Forgez et al. [37]. Heat generation due to contact resistance is also added to the overall heat generation within the cell as given in Eq. (7) [38].

$$Q_{\text{gen}} = i\left(E_0 - V_{\text{batt}} + T\frac{\text{d}U}{\text{d}T}\right) + i^2R_{\text{c}} \tag{7}$$

2.3. Battery pack thermal model

Different types of cooling systems will influence the performance and cost of the battery pack thermal management system. The heat transfer medium could be air, liquid, heat pipes and phase change material (PCM), or a combination of them. The architecture

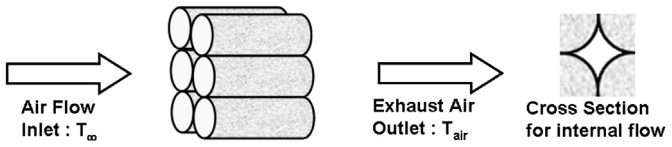

Fig. 3. Schematic of active air cooling system of an EV battery pack [13].

of cooling strategy includes series flow, parallel flow and combination of series and parallel flow. The selection of the cooling system depends on the constraints of the vehicle, installation costs and the external environment. In the extreme environment and working under heavy duty cycles, an active cooling system is preferred to offer more effective thermal management. In this study, parallel air flow strategy is adopted to investigate the thermal response of the battery pack with a certain number of modules. Each module will have the same inlet air temperature that will result in more uniform pack temperature [13] and hence it is sufficient to study a single module in the entire pack. A schematic diagram of the battery pack and the air flow is shown in Fig. 3. The heat transfer coefficient for natural convection and forced convection is defined in Eq. (8) [13,39].

$$h = \begin{cases} h_{\text{forced}} = 30\left(\frac{\dot{m}/\rho_{\text{air}}A_{\text{mf}}}{5}\right)^{0.8} & T_{\text{module}} > 35\ ^\circ\text{C} \\ h_{\text{natural}} = 4 & T_{\text{module}} \le 35\ ^\circ\text{C} \end{cases} \quad (8)$$

2.4. Experimental setup and parameters extraction

Commercial 1.3 Ah 18650 cells with graphite anode coated on the copper current collector, LFP cathode coated on the aluminum current collector, filled with an electrolyte of $LiPF_6$ in EC:DEC 1:1 and Polyvinylidene Fluoride (PVDF) separator were used for experiments. The charging and discharging of the battery was conducted using a battery cycler (Maccor Instrument 4000). According to the procedure followed to Tremblay et al. [33,34], the cell is discharged at 0.2 I_t and the parameters E_0, K, A and B are extracted from the discharge curve shown in Fig. 5(a). The cut off voltage for constant current discharging was 2.3 V. Charging was done in two modes: constant current charging until 4.2 V followed by constant voltage charging until the current dropped to 0.1 A. Before discharging, the cell is charged at 0.1 I_t and followed by 1 h of rest. Slow rate of charging is necessary to ensure that the chemical process within the cell occurs at the similar rate to the transfer of electric energy. Internal resistance (R) of the battery is measured using an impedance analyzer (Solartron analytical 1400). The values of the extracted parameters and other dimensions used in the simulation are provided in Table 1.

Fig. 4. Experimental setup for temperature measurement and the location of thermocouples attached to the surface of the cell.

The surface temperature of the battery was measured using twelve thermocouples (T-type) attached to different locations on the cells. Three thermocouples were attached in the axial direction and four sides of the battery surface as shown in Fig. 4. Measurement of battery surface temperature during charging and discharging at different I_t-rates was done at room temperature of 25 °C under natural convection. All the tests were repeated three times and the average value was taken. Temperature readings were recorded using the HP 34970A data acquisition system. The specific heat capacity of the cell is measured using adiabatic accelerating rate calorimeter (THT ARC). Vehicle specific parameters used for driving cycle simulations are tabulated in Table 2.

2.5. Numerical procedures

The battery and thermal model equations are solved simultaneously in the Matlab-Simulink 2011b. Parameters extracted in Section 2.4 are entered into the battery model in Simulink to investigate the electrical and thermal response of the cell during constant current discharging and SFUDS. Outputs of the simulation model are voltage, current, heat generation and surface temperature of the cell. Heat is dissipated from the cell by natural convection and radiation. The model was validated using constant current discharging experiments ranging from 1 I_t (1.3 A) to 3 I_t (3.9 A) and SFUDS dynamic power profile. Under SFUDS test, the cell is subjected to continuous charging and discharging until its SOC reaches 10%. This validated model was then used to study the thermal response of the battery pack for a converted EV using Hyundai Trajet under UDDS, HWFET and US06 driving cycles that are illustrated in Fig. 1.

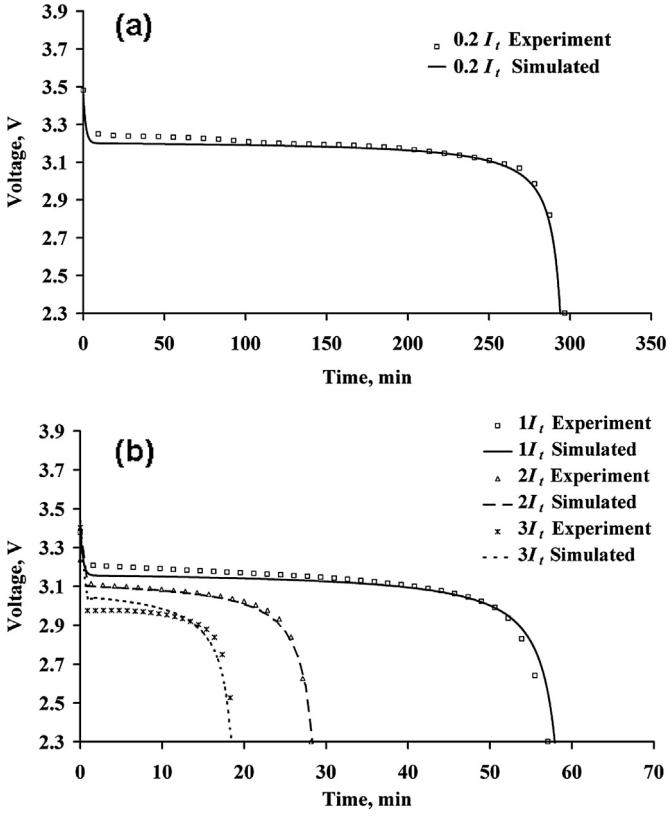

Fig. 5. (a) Model calibration: Cell voltage during discharge at 0.2 I_t to extract the model parameters. (b) Validation of battery model: Cell voltage during discharge at 1, 2, and 3 I_t-rates.

Table 1
LFP cell parameters.

Parameter	Value	Parameter	Value
Nominal voltage, V	3.0	E_0, V	3.21
Nominal capacity, Ah	1.3	R, Ω	0.03
Weight, kg	0.040	K, Ω or V(Ah)$^{-1}$	0.0119
Density, kg m^{-3} [40]	2700	A, V	0.2711
Cathode material	$LiFePO_4$	B, (Ah)$^{-1}$	152.130
Anode material	Graphite	Reference temperature, T_{ref} (K)	298.15
Cell length, m	0.065	Cell diameter, m	0.018
Specific heat capacity, J kg^{-1} K^{-1}	900	Emissivity of heat shrink wrapping, ε [41]	0.95
Stefan–Boltzmann constant, σ (W m^{-2} K^4)	5.67×10^{-8}	Heat transfer coefficient for constant current discharging, W m^{-2} K^{-1} (estimated)	8

3. Result and discussion

3.1. Validation of the cell potential

Discharge characteristics of the cell predicted by the battery model and experimental data are provided in Fig. 5(a). The average squared error of the simulated and measured voltage is about 0.000184. This is followed by comparing the predicted results of the model with the experimental discharge curves at 1, 2, and 3 I_t-rates as shown in Fig. 5(b). The model predictions match well with the experiments with the average squared error of 0.000482, 0.000184 and 0.000752 respectively for the various discharge rates. At 3 I_t of constant current discharging, the maximum capacity of the cell was reduced by 8% less than the capacity at 0.2 I_t (1.3 Ah). The reduction in the cell capacity at high I_t-rates can be explained by Peukert equation as in Eq. (9). The discharge capacity of the cell reduces as the discharge current increases [3]:

$$C_{bp} = T_{dis} \cdot I_{dis}^{k} \tag{9}$$

3.2. Evolution of the cell temperature and heat generation

The average measured and simulated temperature rise of the cell surface at different I_t-rates of discharging is shown in Fig. 6. The temperature of the cell has a positive relationship with the I_t-rates. The sharp rise of the temperature towards the end of discharge was probably due to the polarization effect of the cell. The simulated results agree well with the experimental results. The average squared error between the simulation results and the experiments at 1, 2, and 3 I_t-rates of discharging are 0.00961, 0.00976 and 0.00831 respectively. The measured average temperature rise of the cell at the end of discharging at 1, 2, and 3 I_t-rates is 6.4 °C, 13.9 °C and 20.0 °C respectively. At low I_t-rates of discharging, heat generated from the cell can be effectively dissipated by natural convection and only a temperature rise of less than 10 °C is observed. On the other hand, large amount of heat was generated at 3 I_t and natural convection is not sufficient to dissipate it and keep the battery within the recommended operating temperature range. The total heat generation predicted by modeling at different I_t-rates during discharging is shown in Fig. 7. Large amount of heat is generated towards the end of the discharge. The maximum amount of heat generated for 1, 2, and 3 I_t-rates, is 0.59 W, 1.47 W and 3.14 W per cell respectively.

3.3. Dynamic behavior of the cell under SFUDS

In SFUDS testing cycle, the battery is operated under a repeated 360 s cycle of charging and discharging at certain specific power as shown in Fig. 1. Variation of the current and voltage during the first cycle of the SFUDS profile is shown in Fig. 8(a) and (b) respectively. Maximum current for discharging is about 0.97 A corresponding to a specific power of 79 W kg^{-1}. The average squared error in the experimental data and simulated results of current is 0.000062. The over potential of the cell during the first cycle is high (≈3.3 V) and amount of energy being discharged from the cell is about 1%. The average squared error between the experimental data and simulated results of over potential is found to be 0.0000046.

Thermal response for the battery is studied for more number of repeated cycles until it reaches the cut-off voltage and the predicted average heat generation data is provided in Fig. 9. The average heat generation rate of the cell during 600 min of the SFUDS cycle is relatively small as compared to the constant current discharging and can be neglected. The average heat generated from the first cycle of SFUDS is about -4.6×10^{-4} mJ. Endothermic heat generation is observed during the initial 75 min of the cycle and heat generation rate is gradually reduced as the dynamic charging and discharging process proceeds. Towards the end of the SFUDS cycle, heat generated from the cell contributes to the increase of the overall cell temperature.

The comparison of experimental data and model predictions for the voltage and temperature profile of the cell under 600 min of SFUDS cycle is shown in Fig. 10(a) and (b) respectively. In general, the voltage of the cell decreases with the number of cycles and oscillate in phase. As shown in Fig. 10(a), there is only a small difference between the measured and simulated cell voltages. Substantial amount of heat is generated towards the end of the SFUDS cycle as compared to the initial 6 min of the cycle. Therefore, the temperature of the cell slowly increases at the end of the cycle as shown in Fig. 10(b). The heat generated in the cell can be effectively dissipated by natural convection and cell is kept within safer operating limits. This validated model can now be extended to a battery pack and employed to study the thermal response of it under various driving cycles as discussed in the next section.

3.4. Thermal responses of the battery pack under different driving cycle

The thermal response of the battery pack designed for the converted EV under different driving cycles is provided in Figs. 11–13. A thermostat feature is also included in the Simulink model with a set temperature of 35 °C i.e., air flow from the blower will start only when the temperature of the battery pack rises above this set value. After 35 °C, blower will come in to deliver 5, 10 or 25 CFM of cooling air per module (140, 280 or 700 CFM for a battery pack). The battery pack delivers power for 176 min (7.7 cycles), 69 min (5.4 cycles) and 35 min (3.5 cycles) of UDDS, HWFET and US06 driving cycles respectively before reaching the cut off voltage of 64.4 V. The temperature of the battery pack increased constantly during the cycle and reaches the maximum at the end of the cycle. The heat generated through the UDDS and HWFET cycle is lesser and hence can be effectively dissipated by natural convection. Battery module temperature at the end of the UDDS and HWFET cycle is about 35 °C as shown in Figs. 11 and 12. As shown in Fig. 13, US06 cycle has more aggressive driving profile as compared to UDDS and HWFET cycles. Hence, more energy is charged and discharged to and from the battery pack and consequently more heat is generated. The battery pack is predicted to generate 4.93 MJ of energy on a US06 cycle at 30 °C. As expected, temperature rise of the battery pack is faster in US06 than UDDS and HWFET cycles. The blower is brought to operation at 744 s when the average temperature of the battery pack reaches 35 °C. The average temperature of the battery module at the end of discharge with 5 CFM of cooling air is about 41 °C and maximum temperature rise at the end of the cycle is about 11 °C. In

Table 2
Vehicle and cooling system specific parameters.

Parameter	Value
Vehicle mass, kg	1828
Frontal area, m^2	3.238
Coefficient of drag, Cd	0.35
Electric motor	75 kW, 200 nm max
Battery pack	19.2 kWh
Number of cell per module	180
Number of module	28
A_{mf} per module, m^2	0.00417
A_{sm} per module, m^2	0.662
Mass flow rate of cooling air for battery pack, cfm	140, 280, 700
Surrounding temperature, °C	30

order to cool the battery pack further, 25 CFM of cooling air is blown to dissipate the heat generated and average temperature of the battery module is brought to 36.5 °C. The blower is operating for about 22.65 min of the total duration of the testing. The higher the flow rate of the cooling air, the slower the temperature rise of the battery module but parasitic loss and power consumption will be higher for higher flow rates. Table 3 provides the total energy used for propulsion as well as the energy recovered through regenerative braking for the various cycles. UDDS is an intensive start and stop driving cycle, therefore the total energy used and recovered is highest. The amount of energy recovered through the HWFET cycle represents the highway driving condition and is the lowest among the three driving cycles. The selection of battery cell to build a battery pack is an essential task to optimize performance,

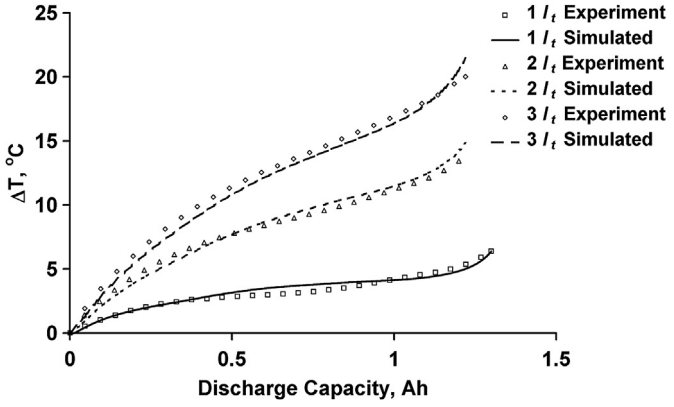

Fig. 6. Temperature rise of the battery during discharge at various I_t-rates.

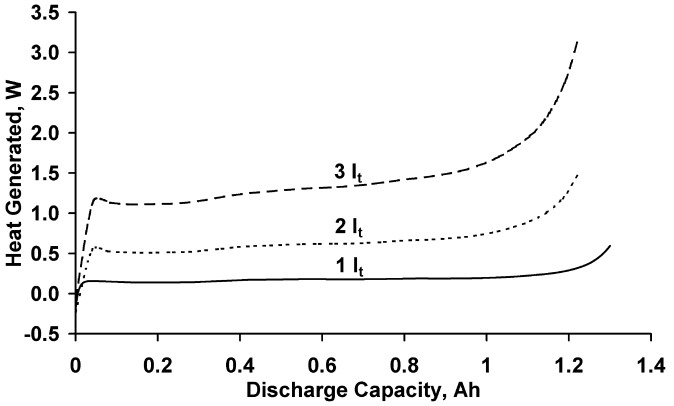

Fig. 7. Heat generation for different I_t-rates of discharging predicted by the model.

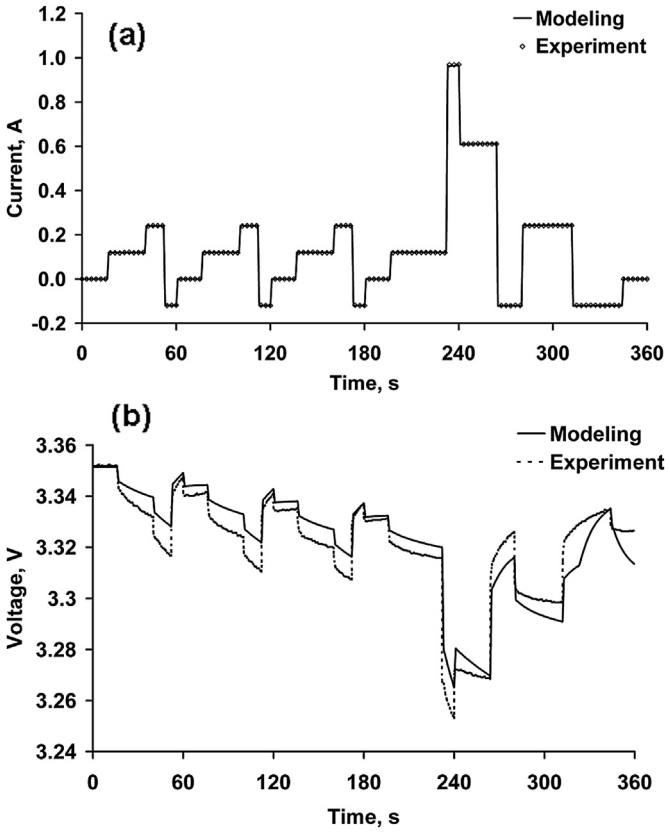

Fig. 8. (a) Current, (b) Voltage during the first 6 min cycle of the SFUDS profile.

prolong the life cycle with affordable cost. Smaller cells are favorable for thermal management and cost effective but high number of electrical connections may result in higher chances of failure and energy lost especially due to contact resistance. Although larger cells (prismatic and pouch cell) offer lower weight and volume efficiency, cost is higher, quality of the cells is not guaranteed and difficult in terms of thermal management. Therefore, a careful consideration is required to select the type of cell to build a battery pack for a certain application.

4. Conclusions

Empirical equation coupled with lumped thermal model is used to predict the thermal performance of the LFP cell under constant current discharging and dynamic charging and discharging cycle.

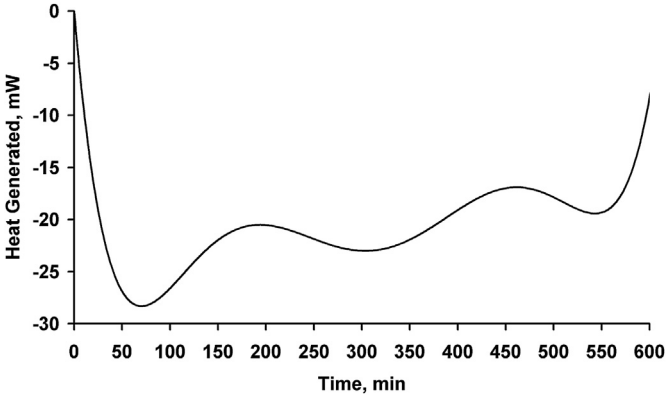

Fig. 9. Average heat generation of the cell during 600 min of the SFUDS cycle predicted by the model.

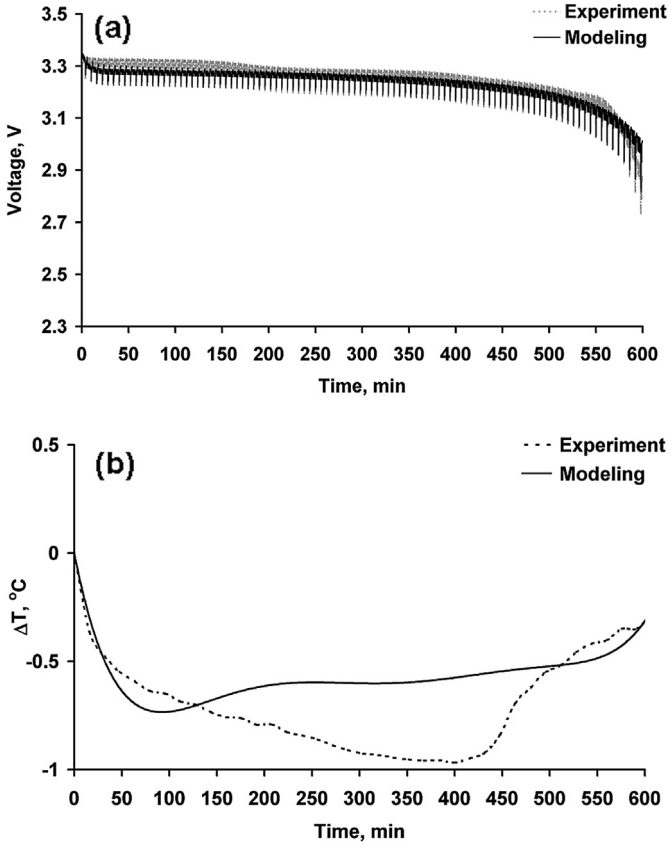

Fig. 10. Comparison of measured and simulated SFUDS profile of a Li-ion cell. (a) Voltage, (b) Temperature.

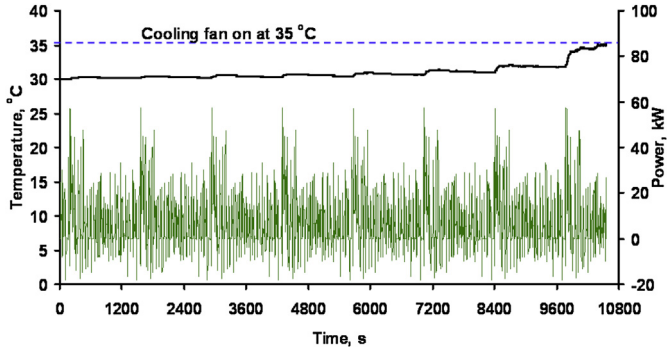

Fig. 11. Thermal response of battery pack to UDDS cycle at 30 °C.

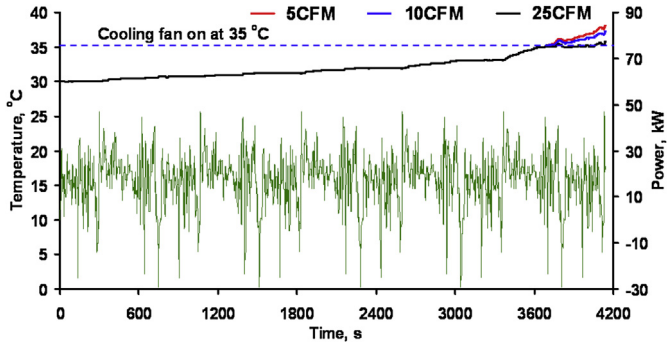

Fig. 12. Thermal response of battery pack to HWFET cycle at 30 °C.

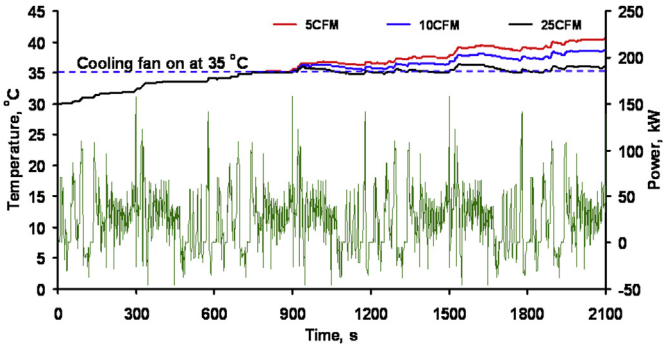

Fig. 13. Thermal response of battery pack to US06 cycle at 30 °C.

Table 3
Energy distribution.

Driving cycle	Discharging, MJ	Charging, MJ	Heat generation, MJ
UDDS	81.91	9.09	0.108
HWFET	73.06	2.17	0.116
US06	58.99	5.71	0.176

Good agreement between the simulated results and experimental data was obtained. The heat generated from the cell increases with increasing I_t-rates. The validated battery model was used to investigate the evolution of the battery pack temperature of a converted EV with different cooling air flow rate under UDDS, HWFET and US06 driving cycles. The heat generated from the battery module is highest for aggressive US06 driving cycle and lowest for the UDDS driving cycle. In a less aggressive driving condition for UDDS and HWFET, natural convection is sufficient to maintain the cell temperature at 35 °C. On the other hand, US06 cycle requires a forced convection cooling (19.0 W m^{-2} K^{-1}) achieved by blowing 700 CFM of cooling air. Hence, a well designed thermal management system is needed for the EV battery pack especially under aggressive driving conditions to ensure safe and reliable operation of the battery pack.

References

[1] Energy Technology Perspectives-scenarios and Strategies to 2050, IEA, 2010. http://www.iea.org/techno/etp/etp10/English.pdf.
[2] P. Van de Bosccche, F. Vergels, J. Van Mierlo, J. Matheys, W. Van Autenboer, J. Power Sources 162 (2006) 913–919.
[3] N. Omar, M. Daowd, P. Van den Bossche, O. Hegazy, J. Smekens, T. Coosemans, J. van Mierlo, Energies 5 (2012) 2952–2988.
[4] T.M. Bandhauer, S. Garimella, T.F. Fuller, J. Electrochem. Soc. 158 (2011) R1–R25.
[5] Report No. DOE/ID 10146EHP Battery Test Working Task Force, USDOE, Aug. 1988.
[6] D.D. Brandt, J. Power Sources 40 (1992) 73–79.
[7] Y. Chen, J.W. Evans, J. Electrochem. Soc. 141 (1994) 2947–2955.
[8] W.B. Gu, C.Y. Wang, B.Y. Liaw, J. Power Sources 75 (1998) 151–161.
[9] K.A. Smith, C.D. Rahn, C.Y. Wang, Energy Convers. Manage. 48 (2007) 2565–2578.
[10] K. Smith, C.Y. Wang, J. Power Sources 160 (2006) 662–678.
[11] G.H. Kim, A. Pesaran, R. Spotnitz, J. Power Sources 170 (2007) 476–489.
[12] G.H. Kim, K. Smith, in: 214th Electrochemical Society Pacific Rim Meeting Honolulu, HI, 2008.
[13] A. Pesaran, J. Power Sources 110 (2002) 377–382.
[14] M.W. Verbrugge, R.S. Conell, J. Electrochem. Soc. 149 (2002) A45–A53.
[15] X. Hu, S. Li, H. Peng, J. Power Sources 198 (2012) 359–367.
[16] P. Nelson, D. Dees, K. Amine, G. Henriksen, J. Power Sources 110 (2002) 349–356.
[17] P. Nelson, I. Bloom, K. Amine, G. Henriksen, J. Power Sources 110 (2002) 437–444.
[18] L. Menard, G. Fontes, S. Astier, Math. Comput. Simul. 81 (2010) 327–339.
[19] D.H. Jeon, S.M. Baek, Energy Convers. Manage. 52 (2011) 2973–2981.
[20] V. Ramadesigan, P.W.C. Northrop, S. De, S. Santhanagopalan, R.D. Braatz, V.R. Subramanian, J. Electrochem. Soc. 159 (2012) R31–R45.

[21] Y. Inui, Y. Kobayashi, Y. Watanabe, Y. Watase, Y. Kitamura, Energy Convers. Manage. 48 (2007) 2103–2109.
[22] L. Cai, R.E. White, J. Power Sources 196 (2011) 5985–5989.
[23] R. Sabbah, R. Kizilel, J.R. Selman, S. Al-Hallaj, J. Power Sources 182 (2008) 630–638.
[24] R. Mahamud, C. Park, J. Power Sources 196 (2011) 5685–5696.
[25] Y. Yang, X. Hu, D. Qing, F. Chen, Energies 6 (2013) 2709–2725.
[26] S. Park, D. Jung, J. Power Sources 227 (2013) 191–198.
[27] A. Jarrett, I.Y. Kim, J. Power Sources 245 (2014) 644–655.
[28] S. Al-Hallaj, J.R. Selman, J. Electrochem. Soc. 147 (2000) 3231–3236.
[29] S.A. Khateeb, S. Amiruddin, M. Farid, J.R. Selman, S. Al-Hallaj, J. Power Sources 142 (2005) 345–353.
[30] K. Somasundaram, E. Birgersson, A.S. Mujumdar, J. Power Sources 203 (2012) 84–96.
[31] L.H. Saw, A.A.O. Tay, in: Proc. ASME 2013 International Technical Conference and Exhibition on Packaging and Integration of Electronic and Phonic Microsystems. Burlingame, CA. USA, 2013.
[32] C.M. Shepherd, J. Electrochem. Soc. 112 (1965) 657–664.
[33] O. Tremblay, L. Dessaint, J. WEVA 3 (2009).
[34] O. Tremblay, in: Vehicle Power and Propulsion Conference. Arlington, TX. USA, 2007.
[35] L. Rao, J. Newman, J. Electrochem. Soc. 144 (1997) 2697–2704.
[36] W. Fang, O.J. Kwon, C.Y. Wang, Int. J. Energy Res. 34 (2010) 107–115.
[37] C. Forgez, D.V. Do, G. Friedrich, M. Morcrette, C. Delacourt, J. Power Sources 195 (2010) 2961–2968.
[38] K.E. Thomas, J. Newman, J. Electrochem. Soc. 150 (2003) A176–A192.
[39] F.P. Incropera, D.P. Dewitt, T.L. Bergman, A.S. Lavine, Fundamentals of Heat and Mass Transfer, sixth ed., John Wiley & Sons, Asia, 2007.
[40] M. Fleckenstein, O. Bohlen, M.A. Roscher, B. Baker, J. Power Sources 196 (2011) 4769–4778.
[41] Mikron, Table of Emissivity of Various Surfaces, 2012. http://www.eng.lbl.gov/~dw/projects/DW4229_LHC_detector_analysis/calculations/emissivity2.pdf.